Easy-to-Build Satellite Beacon Receiver for Propagation Experimentation at Millimeter Bands

Fernando MACHADO [1], Enric VILAR [2], Fernando P. FONTÁN [3], Vicente PASTORIZA [1], Perfecto MARIÑO [1]

[1] Dept. of Electronic Technology, University of Vigo, EEI, Campus Universitario, 36310, Vigo, Spain
[2] Dept. of Electronic and Computer Engineering, University of Portsmouth, Anglesea Building, PO1 3DJ, Hampshire, UK
[3] Dept. of Signal Theory and Communications, University of Vigo, EET, Campus Universitario, 36310, Vigo, Spain

fmachado@uvigo.es, enric.vilar@port.ac.uk, fpfontan@tsc.uvigo.es, vpastoriza@uvigo.es, pmarino@uvigo.es

Abstract. *This paper describes the design and development of a digital satellite beacon receiver for propagation experimentation. Satellite beacons are frequently available for pointing large antennas, but such signals can be used for measuring rain attenuation and other phenomena as, for example, tropospheric scintillation. A fairly inexpensive beacon receiver has been built using off-the-shelf parts. This instrument is not at all bulky making it suitable for easy transportation. This article analyzes the receiver specifications, describes in detail its structure and presents some operational test results.*

Keywords

Satellite beacon receiver, Software Defined Radio, scintillation, rain fade, vegetation attenuation.

1. Introduction

The increasing demand for larger bandwidths for communications applications, not satisfied by the bands currently used, has prompted a growing interest in millimeter wave bands.

Propagation experiments at these new bands are necessary for the characterization of the various tropospheric phenomena which can degrade the transmitted signal [1]-[4]. These measurements allow the development of new accurate tropospheric propagation models. Satellite beacons are frequently available for helping point large antennas and can be used for measuring rain attenuation and other phenomena such as tropospheric scintillation.

The fast evolution of analog-to-digital conversion devices has made it possible to develop radio equipment where the signal is digitized at intermediate frequency level. Thus, these improvements have made faster and cheaper components available allowing the implementation of traditionally analog functions with digital devices. Current progress also includes an increase in processing speed and bandwidth, making it possible to carry out, in real-time, functions unforeseeable some years ago.

Radio systems have benefited from this progress in digital signal processing and conversion techniques allowing more versatile designs. This allows modern day radios to adapt to multiple usages where most of their functionalities are programmable or reconfigurable. A program-defined radio, SDR (Software-Defined Radio), is not limited to a single functionality, but it can be modified to include a new air-interface standard or to operate within a completely different network [5], [6].

This paper describes the design and development of an inexpensive, easy-to-build beacon receiver for the characterization of propagation effects on satellite radio-communication systems. This receiver has been built using off-the-shelf parts and its structure will be described in some detail. The digital beacon receiver allows the study of amplitude fluctuations experienced by a satellite radio-link. Another interesting feature of this receiver is that it is not at all bulky making it suitable for easy transportation and installation. This feature makes it very convenient for other experiments, for example for measuring vegetation attenuation. Vegetation loss can be measured by comparing the signal level when the receiver is first placed in an unblocked location with line-of-sight (LOS) toward the satellite and then set behind a tree or group of trees. The instrument has already been used for this type of application [7].

The preliminary specification and design of the Ka-band front-end, the signal processing and the data recording system were briefly described in [8] in the frame of European COST Action IC0802 (Propagation tools and data for integrated Telecommunication, Navigation and Earth Observation systems) [9], where a receiver development group has been set up (SGMP: Specific Group on Measurements and Products [10]).

Our current work focuses on extending the applicability of the terminal in the recent propagation experiment Alphasat-Aldo, which involves measurements at 20 and 40 GHz. We thus need to incorporate a new receive chain

at 40 GHz and, possibly, an open-loop satellite position following platform [11].

2. The Satellite Beacon Receiver

The beacon receiver to be designed must measure the amplitude fluctuations in the received signal with enough accuracy and dynamic range. Thus, some preliminary calculations are necessary to figure out the expected carrier-to-noise ratio, CNR, and the available dynamic range, DR, for capturing the signal fades and possible enhancements.

In Tab. 1 preliminary link wanted signal and noise budgets are provided for the specific case of HotBird 6 [12] Ka- and Ku-band beacons (Fig. 1 and 2). For these calculations, we assumed typical antenna gains and conservative receiver noise figures, NF. To obtain adequate carrier-to-noise ratio and dynamic range values, the antenna and the low-noise amplifier, LNA, gains must be high, and the receiver noise factor must be sufficiently low.

	Ka Beacon	Ku Beacon
$EIRP_{min}$	9 dBW	8 dBW
$EIRP_{NOMINAL}$ (Europe)	19 dBW	14 dBW
Antenna Gain (G_{ant}) (1 m Ø)	43.9 dBi	39.5 dBi
Free Space Loss (FSL)	210 dB	205.5 dB
Received power at LNA	-117.1 dBm	-122.1 dBm
Receiver Noise Figure (NF_{RX})	4 dB	2 dB
T_{ant} Clear Sky	70 K	50 K
T_{sys} Clear Sky	508.5 K	219.6 K
C/N_0 Clear Sky	54.4 dB-Hz	53.1 dB-Hz
CNR (300 Hz BW)	29.7 dB	28.3 dB
Dynamic Range	19.7 dB	18.3 dB

Tab. 1. Preliminary link budget.

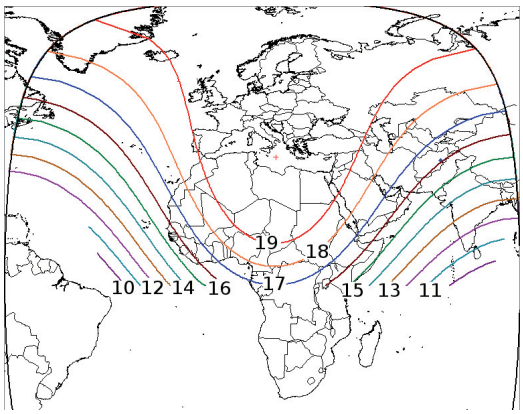

Fig. 1. HotBird6 at 13°E 19 GHz Beacon. EIRP values in dBW.

All calculation, signal and noise, are referred to the antenna port. The next step is to calculate the total noise power which depends on the noise "seen" by the antenna (antenna temperature) [13], and the noise contributed by the receiver, which is mostly due to the LNA if the latter has a sufficient gain. These calculations are reworked in some detail in Section 3.

Finally, the fade margin will depend on the available CNR. For the above preliminary budget we assumed a conventional PLL-based coherent detector [14], [15] with a loop bandwidth, BW, of 300 Hz.

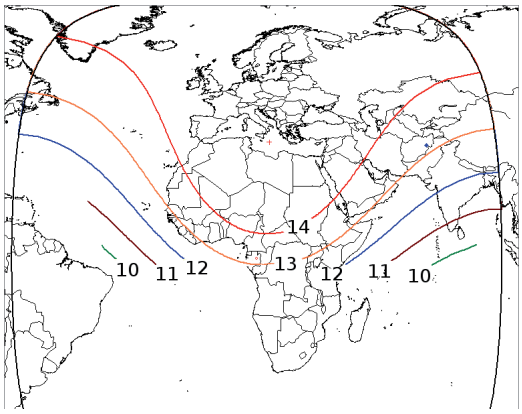

Fig. 2. HotBird6 at 13°E 11 GHz Beacon. EIRP values in dBW.

Additionally, the CNR threshold needs to be at least 10 dB higher, so as not to incur in large amplitude errors. It can be shown that the bias or measurement error, Δ(dB), is a function of the CNR(dB), i.e.,

$$\Delta = 10\log\left(1+10^{-CNR/10}\right). \tag{1}$$

For example, an error target of about 0.4 dB requires a 10 dB CNR. We will use this as our threshold for estimating the signal dynamics we can measure. Therefore, the dynamic range, DR, in the above case is

$$DR(\text{dB}) = CNR(\text{dB}) - 10. \tag{2}$$

Thus, considering that we need at least a minimum CNR of 10 dB to limit the amplitude errors, and the values in Tab. 1 (C/N_0 of about 54 dB-Hz and CNR of about 29 dB, for a loop BW of 300 Hz), the dynamic range in the measurements would be of approximately 19 dB.

With these values, a detector bandwidth of at least 20 Hz would be required for obtaining a dynamic range greater than 30 dB. This range cannot be achieved economically using analog hardware [5].

Satellite beacons are often low-power, unmodulated carriers. These continuous wave (CW) signals are transmitted with constant power and frequency. Thus, we can suppose that the beacon occupies a small bandwidth. However, this wanted signal is accompanied by noise, normally assumed to be white. To facilitate signal detection we need to perform the measurement in the smallest bandwidth possible. In general, signal detection can be performed in two main ways [9]: coherent detection and spectral estimation.

Coherent detection can be achieved using a PLL (Phase-Locked Loop) or an FLL (Frequency-Locked Loop). Phase or frequency tracking accuracy can be enhanced by choosing an adequate bandwidth. Thus, by increasing the loop bandwidth we can improve the tracking performance. However, the CNR threshold increases and consequently the stronger signals can be tracked. On the

other hand, by reducing the loop bandwidth, the CNR threshold decreases meaning that weaker signals can be tracked. Thus, the CNR threshold is reduced at the expense of requiring longer re-acquisition times if the signal goes below the threshold, for example after a deep fade.

For example, for a commercial receiver [15] with a 300 Hz PLL, it is specified that the re-acquisition C/N_0 threshold is 35 dB-Hz, needing around 90 s to reach the locked state (for a VCO sweep of ±200 kHz). This setting is recommended for propagation measurements where the dynamic range is the key requirement. However, with a 2 kHz PLL bandwidth, the re-acquisition C/N_0 threshold is 43 dB-Hz, but requiring less than 1 s to lock (for a VCO sweep of ±200 kHz). This setting is recommended for tracking applications.

An alternative to the above closed-loop detectors is performing open-loop spectral estimation. This can be achieved by performing real-time spectral analysis by means of Fast Fourier Transforms (FFT). In this case, the measurement would involve recording the time evolution of the strongest spectral line(s). The dynamic range in this case is driven by the width of each frequency bin, determined by the number of FFT points. It must be borne in mind that there is always a tradeoff between the dynamic range and the number of power measurements per second.

3. Receiver Structure

The receiver has been built using off-the-shelf elements which have been grouped into three main parts:

A. the RF or outdoor unit,

B. the indoor frequency conversion unit and

C. the signal processing and data logging unit, implemented by means of a radio amateur SW receiver and a PC.

Unlike for the beacon receiver in [6], and in order to use cheaper off-the-shelf parts, a double down-conversion setup was implemented.

Fig. 3 shows a photo of the Ka-Band receiver where a lens-horn antenna on a tripod plus a low-noise block, LNB, converter comprise the *outdoor unit*. This is connected to an *indoor unit*, mainly carrying out frequency conversion and amplification functions. A software radio receiver and a PC complete the instrument performing signal processing and data logging (Fig. 4).

What has been called outdoor unit should provide better measurements if located indoors, close to a window, to prevent accumulation of rain drops on the radome at the horn opening. The window may be fitted with a microwave-transparent material capable of preventing condensation on its surface [16].

A second unit has been developed for receiving a Ku-band beacon. The receiver structure is identical to that used for Ka-band; the only difference is the antenna and the LNB which are specific for that band.

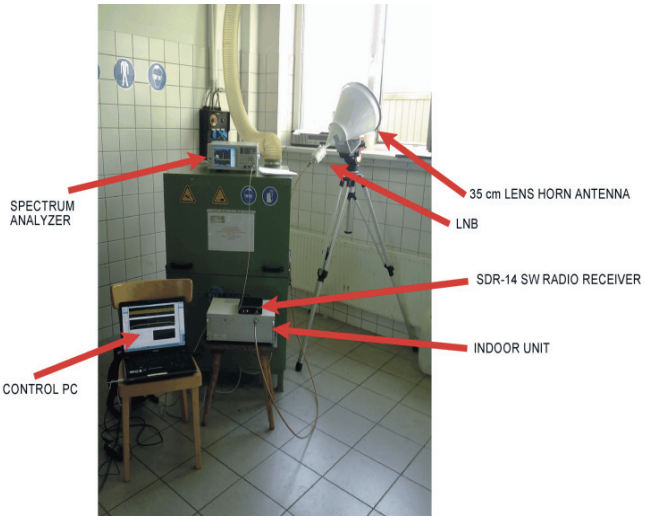

Fig. 3. Photo of the University of Vigo Ka-band beacon receiver.

In Tab. 2 and Tab. 3 summaries of the frequency plans for the Ka- and Ku-band receivers are provided.

Ka-beacon	19701.0 MHz
Ka-band LNB (RF)	19.20–20.20 GHz
Ka-band LNB (IF)	0.950–1.950 GHz
LO_1	18.2500 GHz
IF_1	1451 MHz
LO_2	1440.3 MHz
IF_2	10.7 MHz

Tab. 2. Summary of Ka-band beacon receiver frequency plan.

Ku-beacon	11700.4 MHz
Ku-band LNB (RF)	11.70–12.20 GHz
Ku-band LNB (IF)	0.950–1.450 GHz
LO_1	10.75 GHz
IF_1	950.4 MHz
LO_2	939.7 MHz
IF_2	10.7 MHz

Tab. 3. Summary of Ku-band beacon receiver frequency plan.

3.1 Outdoor Unit

The RF or outdoor unit (A) comprises a lens-horn antenna, manufactured by Flann Microwave [17] (model 20820-XA 350 mm diameter), and a LNB from Norsat [18] (model 9000XBN). The antenna provides a gain of 36 dBi at 19.701 GHz (Ka-band) and its output port is a rectangular waveguide (WR42), which interfaces the LNB. The LNB covers the frequency range 19.20–20.20 GHz, and provides low-noise amplification and block-conversion to the standard 0.950-1.950 GHz satellite receiver IF. This unit has an overall gain of 55 dB and a noise factor of 1.3 dB. The LNB output connector (N-type 50 Ω) is joined to the indoor unit by a low-loss coaxial cable (0.5 dB/m). In addition, through the coaxial cable, also an external 10 MHz clock reference and a 15 V DC voltage are supplied to the LNB (Fig. 4).

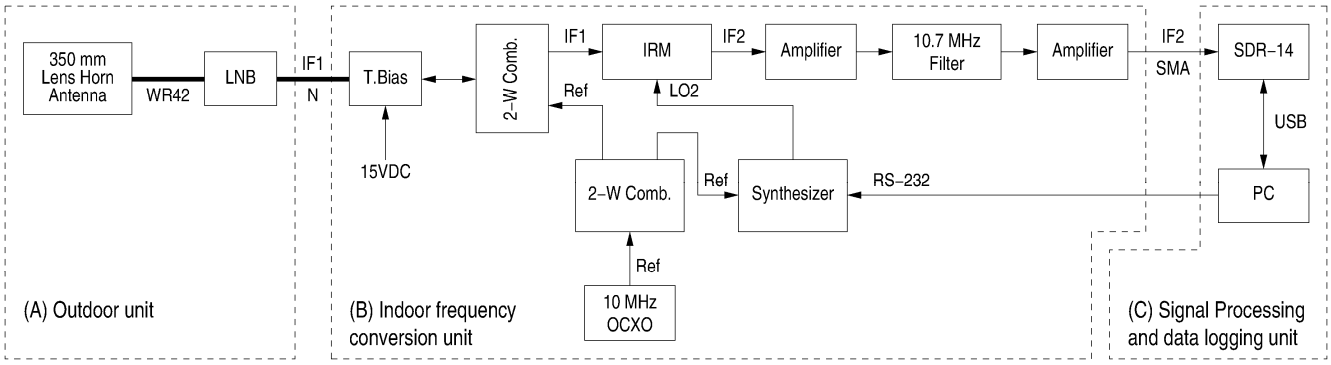

Fig. 4. Receiver's schematic diagram.

For the second receiver, Ku-band, the antenna is again from Flann Microwave (Model 17820-XA 350 mm diameter), which provides a gain of 31.5 dBi at 11.701 GHz; and the LNB is from Norsat [19] (model 1008XAN) with a frequency range of 11.70–12.20 GHz. Its overall gain is 62 dB and its noise figure 0.8 dB. This LNB also requires a 10 MHz clock reference supplied by the indoor unit through a low-loss coaxial cable.

We can now rework the link budget in Tab. 1 using the specifications for the front-end elements in our Ka-band receiver: antenna gain, $G_{\text{ant}} = 36$ dBi, LNB noise figure, $NF = 1.3$ dB, and LNB gain, $G_{\text{LNB}} = 55$ dB.

Thus, considering the HotBird 6 Ka beacon (EIRP = 39 dBm), the received signal at the antenna port/LNB input port is

$$C_{\text{LNB}} = EIRP - FSL + G_{\text{ant}} = -155.43 \text{ dBW} = -125.43 \text{ dBm} . \quad (3)$$

We now calculate the system's noise temperature, also referred to the input port of the LNB. We assume a typical clear sky antenna temperature, $T_{\text{ant}} = 70$ K [13], and supposing that the elements downstream of the LNB do not contribute significantly to the overall noise power, then the system temperature is

$$T_{\text{sys}} = T_{\text{ant}} + T_{\text{RX}} = 70 + T_0 (10^{NF/10} - 1) = 171.2 \text{ K} \quad (4)$$

and the system's noise figure is

$$NF_{\text{sys}} = 10 \log (T_{\text{sys}} / T_0 + 1) = 2 \text{ dB} . \quad (5)$$

The noise power density, N_0, is

$$N_0 = K + 10 \log (T_{\text{sys}}) = -176.26 \text{ dBm/Hz} \quad (6)$$

where K is the Boltzmann's constant (K = -198.6 dBm/Hz/K), which gives

$$C / N_0 = C_{\text{LNB}} - N_0 = 50.84 \text{ dBHz} . \quad (7)$$

Thus, for a resolution bandwidth of 10 Hz,

$$CNR = C / N_0 - 10 \log (BW) = 40.84 \text{ dB} \quad (8)$$

which means that, with the 10 dB threshold, the dynamic range is

$$DR = CNR - 10 = 30.84 \text{ dB} . \quad (9)$$

In the same way, we recalculate the link budget for the HotBird 6 Ku-band beacon using the specifications for the receiver components. The resulting link budgets for both bands are shown in Tab. 4.

HotBird 6	Ka Beacon	Ku Beacon
$EIRP_{\text{min}}$	9 dBW	8 dBW
$EIRP_{\text{NOMINAL}}$ (Europe)	19 dBW	14 dBW
Antenna Gain, (G_{ant})	36 dBi	31.5 dBi
Free Space Loss (FSL)	210 dB	205.5 dB
Received power at LNB (C_{LNB})	-125.43 dBm	-130 dBm
LNB Noise Factor (NF_{LNB})	1.3 dB	0.8 dB
T_{ant} Clear Sky	70 K	50 K
T_{sys} Clear Sky	171.2 K	108.7 K
C/N_0 Clear Sky	50.8 dB-Hz	48.2 dB-Hz
CNR (10 Hz BW)	40.8 dB	38.2 dB
Dynamic Range	30.8 dB	28.2 dB

Tab. 4. HotBird6 link budget.

3.2 Indoor Frequency Conversion Unit

The indoor frequency conversion unit (B) performs further amplification, filtering and frequency conversion to a second IF where analog-to-digital conversion takes place, already at the signal processing and data logging part (C).

A basic element of (B) is a 10 MHz oven-controlled crystal oscillator (OCXO) from Wenzel Associates [20] (Small Fry OCXO model). This OCXO provides not only the required reference for the LNB's internal oscillator, but also it interfaces a 1 kHz step synthesizer from Atlantec RF [21] (model ANS3-0800-001, 800–1200 MHz, 1 kHz steps). The synthesizer is used as the local oscillator for the second IF mixer. The frequency range of the synthesizer is normally not enough to cover all possible beacon frequencies, already down-converted to the first IF at about 1 GHz. Therefore, a specific unit is required depending on the beacon to be received. Still, there is a great flexibility in using this approach, as different beacons in the same general frequency region can be tuned in fairly easily. Thus, two synthesizers have been acquired, one for the Ka-band receiver and another for the Ku-band receiver (model ANS3-1200-001, 1200–2000 MHz, 1 kHz steps). The synthesizers can be controlled from the PC in unit (C) by means of an RS-232 serial port (Fig. 4).

Given that the second IF is quite low, 10.7 MHz, an image reject mixer (IRM) from Polyphase Microwave [22] (model IRM0622B 600–2200 MHz) has been se-

lected. This provides an image frequency rejection of 35 dB which has proven to be sufficient for the application in hand.

The mixer is followed by a band-pass filter centered at the second IF (10.7 MHz). We used an elliptic LC filter from Mini-Circuits [23] (model SBP-10.7+) with a bandwidth of 4 MHz. Two Mini-Circuits 17 dB amplifiers [24] (model ZFL-1000, 0.1–1000 MHz) were used in an amplifier-filter-amplifier setup (Fig. 4).

The amount of amplification is very much dependent on the input levels handled by the analog-to-digital converters of the next element, already in unit (C) and integrated in the software radio receiver devoted to signal processing and data storage.

Unit (B) is also fitted with a number of power supplies for its various modules and also for feeding the LNB through a Bias-T unit [25] (Mini-Circuits ZX85-12G-S+, 0.2–12000 MHz). A number of power splitters/combiners [26] (Mini-Circuits ZFRSC-42B-S+, DC-4200 MHz) have also been included to furnish the LNB and the synthesizer with a common clock reference. Moreover, the second receiver (Ku-band) also uses the reference oscillator of the first one (Ka-band). Fig. 5 shows a photo of the indoor unit.

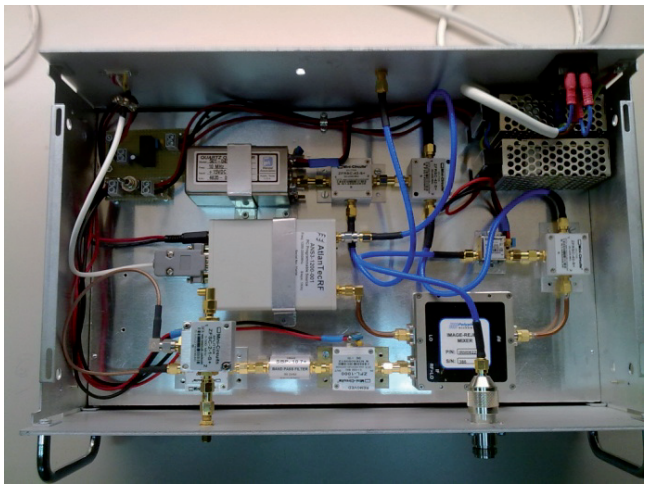

Fig. 5. Photo of the indoor frequency conversion unit.

The overall gain (LNB + indoor frequency conversion unit) comprises the Bias-T insertion loss, $L_{\text{Bias-T}}$, the LNB gain, G_{LNB}, the mixer conversion loss, L_{IRM}, the gains of the amplifiers, G_{AMP}, and the filter insertion loss, L_{Filt}:

$$G = G_{\text{LNB}} + 2 \times G_{\text{AMP}} - L_{\text{Bias-T}} - L_{\text{IRM}} - L_{\text{Filt}} . \quad (10)$$

Considering the gains of the Ka and Ku-band LNBs (55 and 62 dB respectively), the mixer conversion loss (7 dB @ 1400 MHz and 10 dB @ 900 MHz) and the typical values of the Biast-T insertion loss (0.5 dB), the gains of the amplifiers (17 dB) and the filter insertion loss (1.5 dB), the overall gain of the Ka- and Ku-band receivers are G = 80 dB and G = 84 dB, respectively.

3.3 Signal Processing and Data Logging Unit

The signal processing and data logging unit (C) is made up of an amateur radio software receiver from RFspace [27] (model SDR-14) which is driven by a PC. The SDR-14 consists of a 14 bit A/D converter (ADC), a digital down-converter (DDC), and a USB interface [28]. Thus, the SDR-14 performs A/D sampling and a third down conversion to baseband. After that, the I and Q components are passed on to the PC through an USB port. Finally, these signals are processed and stored along with the resulting measurements in the computer. All of the demodulation and spectral functions are carried out on the PC side.

Now we describe in some detail the main characteristics of unit C.

3.3.1 Analog-to-Digital Conversion

The SDR-14 has two selectable input paths going to the ADC: direct input with no filtering or gain, and a 0.1 to 30 MHz filtered path with a programmable preamplifier [27]. The 10.7 MHz second IF signal, from the previous indoor frequency conversion unit, is connected to the pre-amplified, filtered input of the SDR-14. The signal is passed on to the high performance, 14 bit ADC from Analog Devices (model AD6644) running at 66.66667 MSps (mega samples per second). This ADC achieves a typical signal-to-noise ratio of 74 dB considering the A/D quantization, thermal, differential non-linearity (DNL) and jitter noise contributions.

The noise power allowed into the ADC will depend on the bandwidth of the RF/IF chain: Outdoor Unit + Frequency Conversion Unit + Analog SDR-14 input. The bandwidth in this case is limited by the final IF filter which is approximately 4 MHz. Thus, the CNR is

$$CNR = C / N_0 - 10\log(BW) = 50.8 - 10\log(4 \cdot 10^6) = -15.2\text{dBm} . \quad (11)$$

We also need to know whether the RF front-end can handle the received signal plus noise close to the maximum accepted level at the ADC. According to the specifications of the SDR-14, the maximum input is 5 dBm with an ADC signal-to-noise ratio, SNR, of 74 dB (-1 dBm full-scale).

The wanted signal at the ADC input is the signal at the antenna output plus the overall gain, G = 80 dB (10), i.e.

$$C_{\text{ADC}} = C_{\text{LNB}} + G = -125.43 + 84.5 = -45.43 \text{ dBm} . \quad (12)$$

Since C/N_0 is equal to 50.8 dB-Hz, the signal noise level at the ADC input, considering an IF_2 bandwidth of 4 MHz, is

$$N_{\text{ADC}} = C_{\text{ADC}} - C / N_0 + 10\log(BW) = -30.2 \text{ dBm} . \quad (13)$$

It can be observed that the total power at the input of the ADC is dominated by the noise, thus,

$$P_{\mathrm{ADC}} \approx N_{\mathrm{ADC}} = -30.2\mathrm{dBm} \quad (14)$$

which is about 35 dB below the maximum receive level allowed; this permits using most of the dynamic range of the ADC's 14 bits. We still have room to raise the amplification by 20 dB if needed.

3.3.2 Digital Down Conversion

The third down-conversion is performed by the SDR-14 on the digitized 10.7 MHz signal. The 0 Hz and neighboring frequencies must be avoided due to likely interference from the mains power frequency and other sources. Thus, the new 3rd IF is rather kept close to 1 kHz. This digital down conversion provides the I and Q signal components which are passed on to the controlling PC through an USB port. Within the SDR-14 several other filtering and decimation tasks are performed by means of ASIC AD6620 from Analog Devices, whose settings can be selected from the PC. This device carries out the standard functions of a Digital Down-Converter, DDC. These basic functions are: frequency generation, I and Q down-conversion, filtering and decimation.

3.3.3 Digital Signal Processing and Data Logging

The received I and Q components are processed and stored in the PC. The digital signal processing software allows the implementation of different processing methods. Several FFT based methods can be found in [5], [6], [29]-[30]. By changing the number of FFT points, and the sampling rate by decimation, several frequency resolutions and measurement windows can be selected.

In the PC, the received I and Q components are processed by applying a Hanning window before computing an FFT. The FFTs can be performed on non-overlapping sections of the data or on partially overlapping sections, thus increasing the output rate. Thus, rates of the order of 10 Sps (samples per second) or larger can be easily obtained.

The peak FFT frequency bin and two bins on either side are power-summed to compute the received signal variations (Fig. 6). Depending on the selected settings, including the size of the FFT, different sampling frequencies can be achieved. The controlling software has been developed making use of the DLLs supplied by RFSpace [28]. Fig. 7 shows the controlling software user interface from where the receiver settings, measurement file path and other commands can be issued. The I/Q signals, the power spectrum and signal level plots are also presented in the user interface.

The final measurement bandwidth is determined by the sampling rate, the decimation factor, the type of window (Hanning, Hamming, Blackman-Harris, etc.) and the number of FFT points used in the detection of the I/Q signal.

In the implemented default configuration, the received RF signal at Ka/Ku-band is down-converted to

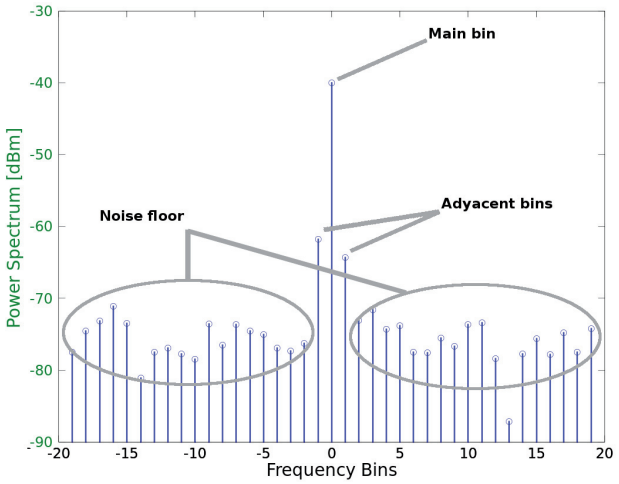

Fig. 6. Spectral estimation of the amplitude (FFT bins).

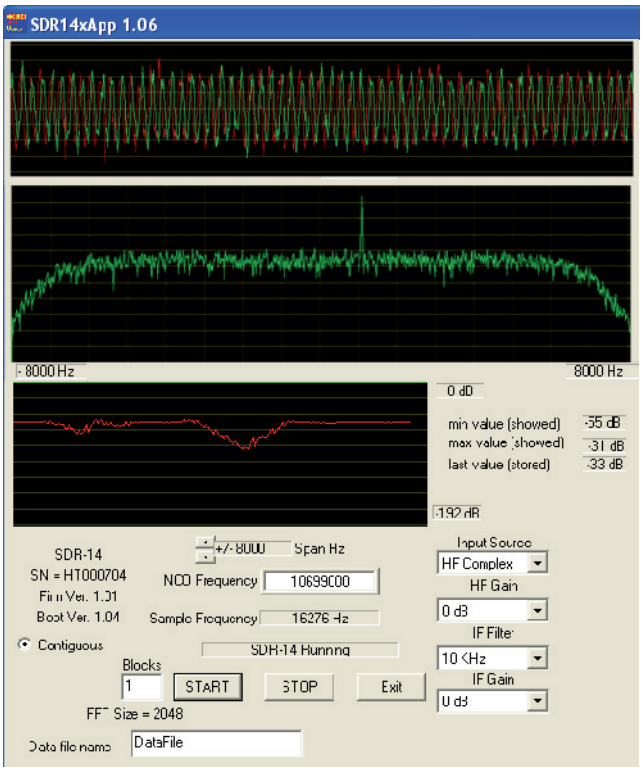

Fig. 7. User interface of the receiver's controlling software.

$IF_2 = 10.7$ MHz, with a bandwidth of 4 MHz. This signal is then sampled with a rate of 66.6667 MSps and converted in the SDR-14 DDC to a center frequency of 1 kHz I and Q signal. The decimation factor within SDR-14 was set to $N = 4096$, which leads to a rate of approximately 16276 Sps. Depending on the number of FFT points used, e.g., 2048/4096/8192, the frequency resolution (FFT bin width or resolution band-width, *RBW*) would be respectively 8/4/2 Hz, with a data rate of 8/4/2 FFT/s, i.e., complex envelope samples per second. With the previous values, considering a Hanning bandwidth increase factor ($B = 1.5$) and the number of power-summed bins ($N = 3$), the measurement bandwidth,

$$MBW = RBW \times N \times B\,, \quad (15)$$

would be of 36/18/9 Hz and the CNR of the measured signal,

$$CNR_{\text{meas}} = C/N_0 - 10\log(MBW), \quad (16)$$

would be of 34/37/40 dB.

The FFT rate can be doubled by using data overlapping while the frequency resolution remains the same. Nevertheless, the above sampling rates are sufficient for the considered phenomenon. For example, the fastest expected signal variations are due to tropospheric scintillations. These are rapid fluctuations caused by random variations in the refractive index of the medium, whose power density is usually only significant for frequencies up to 0.5 Hz [31]-[34]. Since the scintillation's effective bandwidth ($eBW = 1.6 \cdot f_c$) is a function of the so-called corner frequency (f_c), rates in the order of 4 Sps, measurements per second, will allow resolving the high frequency roll-off features present in the signal.

Finally, the signal variations obtained from the FFT analysis can be stored on the PC for later analysis together with the row I and Q signals.

4. Operational Test Results

In this section some operational test results are presented. First, the developed beacon receiver was tested in a laboratory setup to measure linearity and dynamic range. Then, the antenna was pointed to receive the HotBird 6 Ka-band beacon and the second IF signal was split and simultaneously connected to a commercial, open-loop beacon receiver [14] and to the signal processing and data logging unit (C). Thus, we can compare experimental measurements from the developed, open-loop receiver and the commercial, closed-loop one. Finally, we show some experimental results obtained from one of the measurement campaigns where this instrument has been used [35]. These measurements are performed using a 4096 points FFT setup.

4.1 Laboratory Setup

In order to measure the linearity and the dynamic range of the beacon receiver, a laboratory setup was used. Thus, a signal generator was used to provide a first IF ($IF_1 = 1.451$ GHz), continuous-wave signal to the indoor unit.

Considering a received signal in clear-sky conditions $C_{\text{LNB}} = -125.43$ dBm (Tab. 4), and the LNB gain, $G_{\text{LNB}} = 55$ dB, the signal level at the outdoor unit input is $C_{\text{IF1}} = -70.43$ dBm and the signal level at the ADC input is $C_{\text{ADC}} = -42.43$ dBm. Therefore, the power of the signal generator output was set from a level 10 dB over that of clear-sky conditions,

$$C_{\text{IF1max}} = C_{\text{IF1}} + 10\,\text{dB} \approx -60\,\text{dBm}, \quad (17)$$

down to a level 10 dB below the *CNR* of the measured signal,

$$C_{\text{IF1min}} = C_{\text{IF1}} - CNR_{\text{meas}} - 10\text{dB} = -70.43 - 37 - 10 \approx -120\,\text{dBm} \quad (18)$$

in 2 dBm steps.

These measurements were performed first with a clean signal, a pure CW signal, and then with a noisy signal. Thus, considering clear-sky conditions, $C/N_0 = 50.8$ dB-Hz and C_{ADC} (12), the noise density in the second IF signal is set to a value of $N_{0\text{ADC}} \approx -93$ dBm/Hz. Fig. 8 represents the results of these measurements.

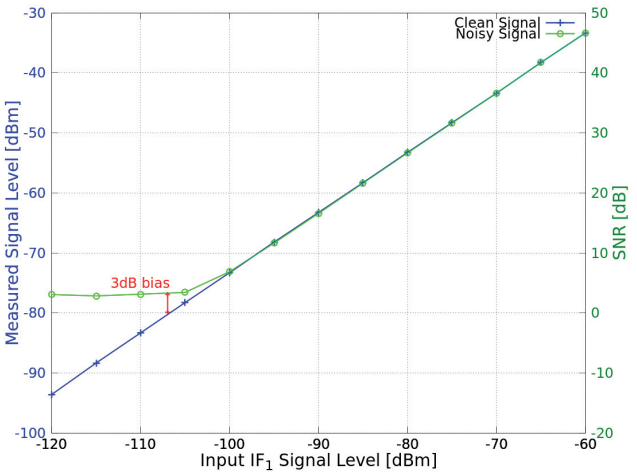

Fig. 8. Digital beacon receiver's linearity curve.

From these results, we can observe that with the clean signal (no noise added) the digital beacon receiver response is linear in the measurement range. Nevertheless, when the simulated noise from the antenna and the receiver is considered, a compression point can be observed when the signal level is near that of the noise. When the measured level equals the noise the 3 dB bias error (1) can be clearly observed (Fig. 8), i.e.,

$$C_{\text{ADC}} = N_{\text{ADC}} = N_{0\text{ADC}} + 10\log(MBW) = -80.4\,\text{dBm}. \quad (19)$$

In order to compare the performance of the developed digital beacon receiver (open-loop, FFT-based) with a commercial closed-loop based one [14], a parallel experimental setup has been used. The signals simultaneously received in both receivers are stored in order to compare and characterize the performance of the digital receiver (Fig. 9). Thus, we can attenuate the received signal by different dB values and compare the dynamic range, C/N_0 threshold and the recovery time after a deep fade.

Fig. 9 shows how the closed-loop receiver requires a minimum C/N_0 threshold is 30 dB-Hz, according to its specifications. Since the clear-sky received signal has a $C/N_0 \approx 50$ dB-Hz, this means that only fades up to approximately 20 dB can be measured. On the other hand, the FFT-based digital receiver has a C/N_0 threshold of 22 dB-Hz (to keep the bias error below 0.4 dB (2)), and a DR of about 28 dB is achieved.

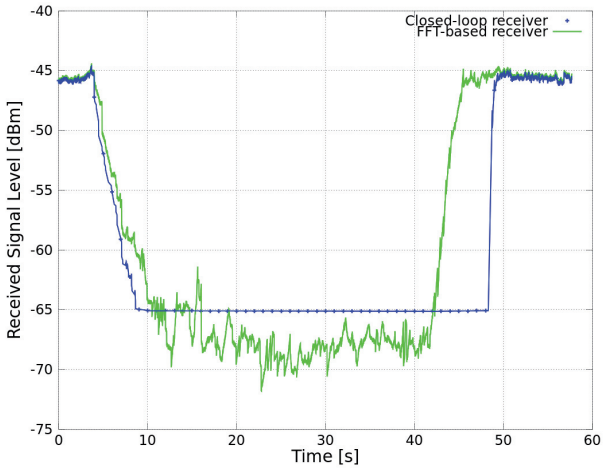

Fig. 9. Comparative experimental measurements from the developed Ka-band closed-loop and the open-loop beacon receiver: DR and reacquisition time.

Moreover, we can observe how after a deep fade the open-loop receiver recovery time is shorter (practically instantaneous) than that of the closed-loop receiver. Thus, after a fade, the closed-loop receiver loses lock and needs several seconds, after the signal goes up again above the threshold level, to recover the lock. Fig. 9 shows how around second 10 the signal goes down the threshold and the closed-loop receiver loses lock (constant signal). Then, around second 15 the signal goes back above the threshold, but the receiver does not recover the lock. It is only when the signal stays over the threshold for about 6 seconds that the closed-loop receiver recovers the lock. However, the FFT-based receiver starts to provide power measurements as soon as the receiver fills up one FFT window (4096 samples), approximately 1/4 s.

4.2 Operational Tests in Austria

At this point, some results obtained from a measurement campaign in Linz, Austria, where this instrument was used [35], are shown. Tab. 5 summarizes the link budget signal and noise experimental measurements in sunny clear-sky after the receiver had been installed in its location and the antenna had been pointed to the HotBird 6 satellite.

HotBird 6	**Ka Beacon**
Received power at LNB (C_{LNB})	-128.9 dBm
Received power at ADC (C_{ADC})	-45.65 dBm
C/N_0 Clear Sky	53.3 dB-Hz
CNR (10 Hz BW)	43.3 dB
Dynamic Range	33.3 dB

Tab. 5. HotBird6 Ka-band signal and noise measurements.

The beacon receiver in this experiment supplied a supplementary recording of the attenuation due to rain and clouds concurrent with mobile Ka-band measurements using a Hercules aircraft to carry the transmitter, flying in circles around the general area where a vehicular receiver was measuring both tropospheric and near environment (buildings, trees, lamp poles, etc.) effects. Mobile measurements of Ka-band satellite beacons are difficult to be carried out given that the dynamic range is small and a less directive antenna is needed on the mobile receiver side.

Fig. 10 illustrates a convective event that took place in Linz, Austria [35].

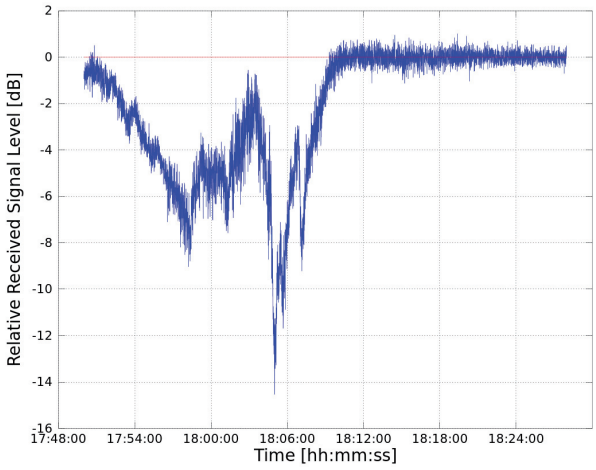

Fig. 10. Example of a convective event measured in Linz, Austria.

5. Summary

In this paper, the design of two beacon receivers for Ka- and Ku-band built for carrying out propagation studies have been presented in some detail. The receivers are quite inexpensive even though they have been built using off-the-shelf parts. This has the advantage of using well proven elements, thus reducing the risk of malfunction. The two receivers share a single reference clock and controlling PC. The digital signal processing part has been implemented on an amateur SW radio receiver; this provides a great flexibility to the design allowing easy changes in the used algorithms.

The availability of fairly cheap and easily programmable hardware makes it possible that satellite beacons can be monitored easily around the world, thus helping characterize the rain attenuation phenomena which is extremely different between climatic zones.

Expected further work will involve the measurement of the cross-polar effects by introducing additional receiver chains to the setup. Additionally, duplicating the receivers, space/site/orbit diversity experiments can also be addressed.

Future plans involve developing two radiometers using the same receive chains as for the Ka and Ku-band beacon receivers, as in [5], by measuring the background noise changes on both sides of the beacons.

Acknowledgements

Fernando Machado would like to thank Prof. Armando Rocha, for assisting him in the study of detection

methods and his advice during the author's stage in the University of Aveiro, Portugal.

References

[1] PARABONI, A., MAURI, M., BARBALISCIA, F., GIANNONE, B. First propagation measurements at 20, 40 and 50 GHz obtained in the framework of the ITALSAT experiment. In *Proc. URSI Open Symposium on Wave Propagation and Remote Sensing*. Ravenscar (U.K.), June 1992.

[2] CASTANET, L., DOUCHIN, N., LEMORTON, J., COLAS DES FRANCS, R., LE BOULCH, D., GRELY, S. Modelling and measurement of radiowave propagation on Earth-satellite links in the millimetre band. In *Proc. AGARD/SPP Symposium*. Athens (Greece), Sep. 1995.

[3] DOUCHIN, N., LEMORTON, J., SAUVAGEOT, H., MARSAULT, T. Experimental study of radiowave propagation effects in the millimetre waves band. In *Proc. 10th International Conference on Antennas and Propagation*. Edinburgh (U.K.), Apr. 1997.

[4] MACHADO, F., VILAR, E., FONTÁN, F. P. A very short distance dynamic diversity experiment. In *Proc. European Conference on Antennas and Propagation, EuCAP 2006.* Nice (France), Sep. 2006, p. 1-6.

[5] KIKKERT, C. J., KENNY, O. P. A digital signal processing based Ka band satellite beacon receiver/radiometer. In *Proc. IEEE International Conf. on Signal Processing and Communication – ICSPC*. Gold Coast (Australia), Dec. 2008, p. 1-8.

[6] MACHADO, F., VILAR, E., MARIÑO, P., FONTÁN, F. P., BLARZINO, G., CARRIE, G., CASTANET, L., LEMORTON, J. Beacon receiver developments at U. Portsmouth-U. Vigo and ONERA. In *2nd SatNex Workshop*, DLR. Oberpfaffenhofen (Germany), Apr. 2008.

[7] JEANNIN, N., FONTÁN, F. P., MAMETSA, H. J., CASTANET, L., LACOSTE, F. Physical-statistical model for the LMS channel at Ku/Ka band. In *Proc. 5th European Conference on Antennas and Propagation, EuCAP 2011*. Rome (Italy), Apr. 2011.

[8] MACHADO, F., NAVEIRAS, D., MARIÑO, P., FONTÁN, F. P. An inexpensive satellite beacon receiver for propagation experimentation at Ka-band. In *COST Action IC0802, Propagation Tools and Data for Integrated Telecommunication, Navigation and Earth Observation Systems*, ISEA. Toulouse (France), Nov. 2009, p. 1-6.

[9] ROCHA, A., SOUSA, M., MACHADO, F., FONTÁN, F. P. Beacon receivers and digital detectors solutions for Earth-satellite propagation campaigns. In *Proc. 6th European Conference on Antennas and Propagation, EuCAP 2012.* Prague (Czech Republic), Mar. 2012.

[10] COST ACTION IC0802. *Propagation Tools / Data for Integrated Telecom, Navigation and Earth Observation*. [Online] Cited 2013-06-10. Available at: http://www.tesa.prd.fr/cost/sgmp.html

[11] CODISPOTI, G., RIVA, C., RUGGIERI, M., ROSSI, T., MARTELLUCCI, A., RIVERA-CASTRO, J., KOUDELKA, O., SCHOENUBER, M. The propagation and telecom experiments of the Alphasat Aldo payload (TDP5 Q/V band experiment). In *Proc. 6th European Conference on Antennas and Propagation, EuCAP 2012.* Prague (Czech Republic), Mar. 2012.

[12] Eutelsat*, Satellite Data Sheet: The Hot Bird 6 Satellite*, Dec. 2005.

[13] MARZANO, F. S., MONTOPOLI, M. Millimeter-wave antenna noise temperature due to rain clouds: Theoretical model and statistical prediction. In *3rd European Conference on Antennas and Propagation, EuCAP 2009*. Berlin (Germany), 23-27 March, 2009, p. 2906-2910.

[14] Matra Marconi Space, *Matra Marconi Space SBR 100. User Guide and Specification.*

[15] Novella, *Beacon Tracking Receiver Technical Notes.* [Online] Cited 2013-06-10. Available at: http://www.novella.co.uk/beacon_tech.htm

[16] KOLLER, D., EDISS, G. A., KERR, A. R. *Dielectric Constant of Goretex RA7956/7957 Radome Material in the Frequency Range 1 MHz-2 THz, ALMA Memo #309*, May 2000. 6 pages. [Online] Cited 2013-06-10. Available at: http://www.alma.cl/almamemos/100214/memo309.pdf

[17] Flann Microwave, *Lens Horn Antennas*. 5 pages. [Online] Cited 2013-06-10. Available at: http://www.flann.com/Products_Home /Antennas/ Lens_Horn/FmiCat078085.pdf

[18] Norsat International Inc., *LNB Ka-Band Ext. Ref 9000X (datasheet)*. 1 page. [Online] Cited 2013-06-10. Available at: http://www.norsat.com/wp-content/uploads/9000x_lnb.pdf

[19] Norsat International Inc., *LNB KU-Band Ext. Ref. 1000X (datasheet)*. 1 page. [Online] Cited 2013-06-10. Available at: http://www.norsat.com/wp-content/uploads/1000xh_lnb2.pdf

[20] Wenzel Associates Inc., *Small Fry OCXO (datasheet)*. 1 page. [Online] Cited 2013-06-10. Available at: http://www.wenzel.com /pdffiles1/Oscillators/SF.pdf

[21] AtlanTecRF. *PC Programmable Sources. ANS3 Series (datasheet)*. 1 page. [Online] Cited 2013-06-10. Available at: http: //www.atlantecrf.com/pdf_downloads/Oscillators/PC%20Programmable%20Sources/PC_Programmable_Sources_ANS3_Series.pdf

[22] Polyphase Microwave. *IRM622B Image-Reject Mixer 600-2200 MHz (datasheet)*. 2 pages. [Online] Cited 2013-06-10. Available at: http://www.polyphasemicrowave.com/datasheets/IRM0622B.pdf

[23] Mini-circuits. *Bandpass Filter. SBP-10.7 (datasheet)*. 1 page. [Online] Cited 2013-06-10. Available at: http://www.minicircuits.com/pdfs/SBP-10.7.pdf

[24] Mini-circuits. *Amplifier ZFL-1000 (datasheet)*. 2 pages. [Online] Cited 2013-06-10. Available at: http://www.minicircuits.com/pdfs/ZFL-1000.pdf

[25] Mini-circuits. *Bias-Tee ZX85-12G (datasheet)*. 2 pages. [Online] Cited 2013-06-10. Available at: http://www.minicircuits.com/pdfs/ZX85-12G+.pdf

[26] Mini-circuits. *Power Splitter/Combiner ZFRSC-42 (datasheet)*. 1 page. [Online] Cited 2013-06-10. Available at: http://ww.minicircuits.com/pdfs/ZFRSC-42+.pdf

[27] RF Space. *SDR-14. Software Defined Receiver & Spectrum Analyzer*. 10 pages. [Online] Cited 2013-06-10. Available at: http://www.rfspace.com/support_files/SDR-14_manual.pdf

[28] Moetronix, *SDR-14 Interface Specification, ver. 1.02, Apr. 2012*. 19 pages. [Online] Cited 2013-06-10. Available at: http://www.moetronix.com/files/sdr14interfacespec102.pdf

[29] HOLM, S. Optimum FFT-based frequency acquisition with application to COSPASSARSAT. *IEEE Trans. on Aerospace and Electronic Systems*, Apr. 1993, vol. 29, no. 2, p. 464-475.

[30] ANGRISANI, L., D'APUZZO, M., VADURSI, M. Power measurement in digital wireless communication systems through parametric spectral estimation. *IEEE Trans. on Instrumentation and Measurement*, Aug. 2006, vol. 55, no. 4, p. 1051-1058.

[31] MOULSLEY, T. J., VILAR, E. Experimental and theoretical statistics of microwave amplitude scintillations on satellite down-links. *IEEE Trans. on Antennas and Propagation*, Nov 1982, vol. 30, no. 6, p. 1099-1106.

[32] VILAR, E., FILIP, M. Measurements of 20/30 GHz amplitude scintillations. Dependence of the statistics upon the ground station

measuring parameters. In *Proc. Olympus Utilisation Conf.* Vienna, (Austria), Apr. 1989, p. 191–197. (ESA SP-292, May 1989).

[33] AMAYA, C., NGUYEN, T., ROCHA, A., RIERA, J. M., BENARROCH, A., GARCÍA-DEL-PINO, P., GARCÍA-RUBIA, J. M., CARRIE, G., CASTANET, L. Joint results of 20 GHz recent earth-space propagation experiments in Canada and Europe. In *Proc. 5th European Conference on Antennas and Propagation, EuCAP 2011*. Rome (Italy), Apr. 2011.

[34] MANDEEP, J. S. Extracting of tropospheric scintillation propagation data from Ku-band satellite beacon. *Int. Journal of Physical Sciences*, June 2011, vol. 6, no. 11, p. 2649-2653.

[35] SCHÖNHUBER, M., TESCHL, F., HOVINEN, V., KYRÖLÄINEN, J., FONTÁN, F., PRIETO-CERDEIRA, R. An experiment and preliminary results for narrow- and wideband land mobile satellite propagation at K-band. In *Proc. 4th European Conference on Antennas and Propagation*, *EuCAP 2010*. Barcelona (Spain), Apr. 2010.

About Authors ...

Fernando MACHADO was born in Vigo, Spain. He received his M.Sc. degree in Telecommunications Engineering in 2000 from the University of Vigo, Vigo, Spain, and his Ph.D. in 2008 from the same university. In 2001 he became an Assistant Professor in the Electronic Technology Department, University of Vigo. Since 2009, he has been an Associate Professor in the same department. He is currently a researcher with the Digital Communications and Instrumentation Group (TE3), University of Vigo. His main research interests include distributed electronic instrumentation, multi-sensor networks, wireless communications, and radio communication systems.

Enric VILAR was educated at the Horta Salesian School of Barcelona, Spain. He received the degree in Physics from the University of Barcelona, the Doctorate in Electronics from the University of Paris, France, and the Ph.D. degree from the University of London, U.K., in 1972. He did research for two years at the Ionospheric Research Group of CNET Labs in Issy-les-Moulineaux, Paris, one year at ESTEC (ESA), Holland, and was with the Alcatel-Standard Electrica Labs (formerly ITTLS), Madrid, Spain, for three years. He has also been Manager of the electronics group of Schlumberger (formerly Compagnie des Compteurs), Barcelona, for two years in the late 1960s. He joined the University of Portsmouth, Portsmouth, U.K., in 1975, founding the Microwave Telecommunication Systems (MTS) research group, and has held the Chair of Telecommunication Systems since 1985. He is currently emeritus professor with the School of Engineering in the University of Portsmouth. Dr. Vilar is a Fellow of the IEE and a member of the Royal Academy of Sciences and Arts of Barcelona. His past interests have included LOS and trans-horizon propagation, satellite radio propagation (from OTS to ITALSAT) for communications and remote sensing, and measurement and characterization of precipitation rate and of phase noise in oscillators. Recently, he initiated and is involved with the characterization and measurement of the wideband radio communications channel. This area runs parallel with the effects of precipitation (fading and interference) into millimeter-wave radio communications operating in urban and suburban environments.

Fernando P. FONTÁN was born in Villagarcía de Arosa, Spain. He obtained his degree in Telecommunication Engineering in 1982 from the Technical University of Madrid and his PhD in 1992 from the same university. After working in industry since 1984 he became an Assistant Professor at the University of Vigo in 1988. In 1993 he became an Associate Professor and in 1999 a Full Professor at the Signal Theory and Communications Department of the University of Vigo. He is the author of a number of books and journal papers and has been the leader in several projects funded by public and private entities. He participates in ITU-R WG3 on Propagation Modeling. He has been a Management Committee Member of EU' COST 255, 280 and 297, and currently participates with the same role in COST IC0802. His main research interest is in the field of mobile fixed radio communication propagation-channel modeling.

Vicente PASTORIZA was born in Bueu, Spain. He received the M.Sc. degree in Industrial Engineering and the Ph.D. degree from the University of Vigo, Vigo, Spain, in 1998 and 2008, respectively. In 2000 he joined the Electronic Technology Department, University of Vigo, as an Assistant Professor; since 2011, he has been an Associate Professor there. He is currently a researcher with the Digital Communications and Instrumentation Group (TE3), University of Vigo. His main research activities are in the fields of atmospheric propagation in radio communication systems, signal processing, and computational intelligence, and their application in decision making and system modeling.

Perfecto MARIÑO received the Ph.D. degree in Telecommunications Engineering from the Polytechnic University of Madrid, Spain, in 1984. He was an Associate Professor with the Electronic Technology Department, University of Vigo, Spain from 1978 to 1993. In 1988, he was a Visiting Scientist in the Computer Science Department, Carnegie Mellon University, Pittsburgh, PA, USA. Since 1993, he has been a Full Professor in the Electronic Technology Department, University of Vigo. His main research interests include distributed electronic instrumentation, wireless sensor networks, fieldbus technology for industrial control, and artificial vision. He was technical co-chair for such international conferences as IECON, ISIE, SIECI, CAIP, CONTROLO, SAAEI, and evaluator of several journals, such as *Mechatronics*, *IEEE Transactions on Industrial Electronics*, *IEEE Transactions on Industrial Informatics*, CIT, ESIME, Elsevier, and others. He is also the Director of the Digital Communications Division of the Electronic Technology Department, University of Vigo. He has been distinguished as an Expert on Information Technology from the Commission of the European Union for the SPRINT (Luxembourg, 1991); COPERNICUS (Brussels, 1994); and ACTS (Brussels, 2002) programs. He has served as General Manager of the Information Society (2002–2004)

and Communications Technology (2002–2006) programs from the State R&D Office (Autonomous Government, Galicia, Spain). He is also an expert from the R&D National Program (Ministry of Education and Science, Madrid) in the evaluation of research projects in the field of information and communication technologies.